Isotope Effects on Zonal Flows and Turbulence in Helical Configurations with Equilibrium-Scale Radial Electric Fields

T.-H.Watanabe[1,2], H.Sugama[1,2], and M. Nunami[1]

[1]National Institute for Fusion Science, Toki, Gifu, 509-5929, Japan
[2]The Graduate University for Advanced Studies, Toki, Gifu, 509-5929, Japan

e-mail contact of main author: watanabe.tomohiko@nifs.ac.jp

Abstract. Isotope effects on zonal flow response and the ion temperature gradient (ITG) instability in magnetically-confined plasma with helical configurations are investigated by gyrokinetic simulations. Poloidally global simulations of the collisionless zonal flow damping manifest enhancement of the residual amplitude by the equilibrium-scale (uniform and constant) radial electric field (E_{r0}), and show agreement with the zonal flow response kernel analytically derived from the theory for helical plasmas with multiple-helicity confinement field components. The higher zonal flow response is found with heavier ion mass for the same ion temperature (T_i) and E_{r0}, because effects of the radial electric field are introduced in terms of the poloidal Mach number (M_p), while the ITG mode frequency is Doppler-shifted. Accordingly, the isotopic dependence of the zonal flow response through E_{r0} leads to the mass (or M_p) dependence of the turbulent transport.

1. Introduction

A variety of isotope effects on anomalous transport have been reported from various fusion plasma experiments but remain to be resolved [1]. Conventional gyrokinetic theory and simulations of the local plasma turbulence predict the gyro-Bohm scaling of transport coefficients showing transport enhancement as the square root of the ion atomic mass number, while several experiments exhibit the confinement improvement in deuterium discharges.

Recent theoretical, numerical, and experimental investigations on the anomalous transport shed a highlight on roles of self-generated poloidal shear flows, zonal flows (ZFs), in regulating the plasma turbulence [2]. ZFs generated by the ion temperature gradient (ITG) turbulence [3] lead to the ion heat transport reduction and the up-shift of critical ion temperature gradient [4]. For finding further reduction of the turbulent transport, the ZF response function [5] has been investigated in detail for effects of collisional [6], plasma shaping [7], short wavelength [8–10], and non-axisymmetric geometry [11–16]. Influences of the radial electric field on the ZF response are recently studied for a tokamak pedestal region [17] and non-axisymmetric (helical) systems [18–20].

Gyrokinetic theory for a helical plasma with an equilibrium-scale radial electric field (E_{r0}) recently predicts enhancement of the ZF response [18–20], where E_{r0} drives the poloidal rotation of helical-ripple-trapped particles with reduced radial displacements of drift orbits [14]. The E_{r0} dependence of the ZF response is regarded as the isotope effect if the ion temperature and the radial electric field are the same for the different ion mass. A neoclassical transport analysis for the Large Helical Device (LHD) [21] confirms that magnitude of the equilibrium radial electric field expected in the deuterium discharge is almost identical to that in the hydrogen plasma if other parameters are the same [22]. An isotope effect on ZF response, thus, appears through E_{r0} generated by the neoclassical transport, and is expected to play a favorable role in reducing the turbulent transport.

In the present study, we investigate isotope effects on the ZF response and the ITG instability in helical plasmas with the equilibrium scale radial electric field, utilizing the gyrokinetic simulation code, GKV [23–25], with extension of the field-line-label dependence of the confinement field and the poloidal rotation due to E_{r0}. A detailed parameter study of the ZF response

for M_p and the radial wavenumbers is shown in the next section, where we examine two helical field structures of the LHD type configuration, that is, the single-helicity and the inward-shifted model cases. The gyrokinetic simulation of the ITG instability is shown in section 3, where we employ a newly-extended GKV code with the field-line-label dependence of the drift and mirror force terms. The uniform and constant E_{r0} leads to the Doppler shift of the ITG mode frequency while the instability growth rate is expected to be unaffected. A nonlinear GKV simulation also presents reduction of turbulent fluctuation levels and transport flux in case with E_{r0}. Accordingly, the isotopic dependence of the zonal flow response through E_{r0} leads to the mass (or, equivalently, M_p) dependence of the turbulent transport. The results are summarized in the last section.

2. Gyrokinetic Simulation of Zonal Flow Response with Radial Electric Field

The first gyrokinetic simulation of the ZF enhancement by E_{r0} in helical systems was carried out by means of the GKV code, and shows increase of the ZF response for relatively large M_p-values in the single-helicity LHD-type configuration [26]. A preliminary report of the GKV simulation for multiple-helicity configuration is given in [20]. Global gyrokinetic simulations for LHD and Wendelstein 7X configurations also demonstrate the enhancement of the residual ZF level by the equilibrium radial electric field Ref. [27]. In this section we describe the GKV simulation results of the ZF response for different M_p and radial wavenumbers for the single and the inward-shifted model configurations of LHD.

2.1 Theoretical Background

In the non-axisymmetric systems, the equilibrium radial electric field E_{r0} drives the poloidal rotation of helical-ripple-trapped particles with reduced radial displacements of drift orbits [14]. Theoretical analysis of the zonal flow response including collisionless orbits for passing, toroidally-trapped, helically-trapped and transition particles predicts the residual zonal flow potential of

$$\phi(t) = \phi(0)/[1 + G_p + G_t + M_p^{-2}(G_{ht} + G_h)(1 + T_e/T_i)] \,, \tag{1}$$

in the long time limit of $t \to \infty$ [19]. Here, G_p and G_t mean the dimensionless geometrical factors related to passing and toroidally-trapped particles. The unclosed and closed orbits of helically-trapped particles are represented by G_{ht} and G_h, respectively. The poloidal Mach number is given by $M_p = |(R_0 q/r_0)(cE_{r0}/B_0 v_{ti})|$, where R_0, r_0, q and $v_{ti} = \sqrt{T_i/m_i}$ denote the major and minor radii, the safety factor, and the ion thermal speed, respectively.

The above response analysis predicts enhancement of the residual flow by increase of M_p, while the shielding effect of the zonal flow potential due to the helically-trapped particles increases for smaller $|k_r|$ in case without E_{r0} [11, 12].

2.2 Simulation Model

Here, we choose the field aligned coordinates of $x = r - r_0$, $y = r_0[\theta - \zeta/q(r)]$, and $z = \zeta$, where the field-line-label $\alpha = \theta - \zeta/q = y/r_0$ is chosen to be $\boldsymbol{B} = (2\pi)^{-1}\nabla\Psi_t \times \nabla\alpha$. The safety factor is denoted by q. The magnetic field strength is given by

$$B = B_0 \left\{ 1 - \varepsilon_{00}(r) - \varepsilon_t(r)\cos(\alpha + z/q) - \sum_l \varepsilon_l(r)\cos[l\alpha + (l/q - M)z] \right\} \,, \tag{2}$$

where the α dependence of the confinement field is explicitly taken into account. For LHD, the toroidal and main poloidal period numbers of the confinement field are $M = 10$ and $L = 2$, respectively.

We solve the linearized gyrokinetic equation describing the collisionless damping of ZFs in the model LHD configuration with the equilibrium-scale radial electric field E_{r0},

$$\frac{\partial \delta f}{\partial t} + v_{\parallel} \boldsymbol{b} \cdot \nabla \delta f + v_{dx} \frac{\partial \delta f}{\partial x} - \mu \left(\boldsymbol{b} \cdot \nabla \Omega_i \right) \frac{\partial \delta f}{\partial v_{\parallel}} + \omega_{\theta} \frac{\partial \delta f}{\partial \alpha} = -v_{dx} \frac{e}{T_i} \frac{\partial \langle \Phi \rangle}{\partial x} F_M \tag{3}$$

where δf, μ, Ω_i, and T_i denote the perturbed ion gyrocenter distribution function, the magnetic moment ($\mu \equiv v_{\perp}^2 / 2\Omega_i$), the ion gyrofrequency, and the ion temperature, respectively. The poloidal $\boldsymbol{E} \times \boldsymbol{B}$ rotation frequency is denoted by $\omega_{\theta} = -cE_{r0}/r_0 B_0$. The ZF component of the electrostatic potential in Eq. (3) is defined by the flux surface average, $\langle \Phi \rangle$.

The electrostatic potential perturbation is obtained by solving the quasi-neutrality condition that is simplified as

$$\frac{e \langle \phi_{k_x} \rangle}{T_i} = \frac{\langle \delta n_{k_x}(y,z) \rangle}{n_0 (1 - \Gamma_0|_{k_y=0})} \tag{4}$$

where $\Gamma_0 = e^{-b} I_0(b)$ with $b = (k_{\perp} v_{ti}/\Omega_{i0})^2$ for $k_y = 0$. The zeroth-order modified Bessel functions is denoted by I_0. The weak dependences on α and ζ of the arguments for J_0 and Γ_0 are ignored by using Ω_{i0} instead of Ω_i, since the difference causes higher-order corrections only. Then, one finds $\langle \Phi_{k_x} \rangle = J_0|_{k_y=0} \langle \phi_{k_x} \rangle$.

We consider two magnetic field structures, that is, the single helicity and the inward-shifted model cases for the LHD configuration. In the former, the main helical field component of $l = L = 2$ is introduced with the toroidal one, where the relative amplitude is set to be $\varepsilon_L = \varepsilon_t = 0.1$. In the latter, side-band components of the helical field are included with the amplitudes of $\varepsilon_{L-1}/\varepsilon_t = -0.8$ and $\varepsilon_{L+1}/\varepsilon_t = -0.2$ with $\varepsilon_L = \varepsilon_t = 0.1$.

2.3 Simulation Results of Zonal Flow Response

Time-histories of the ZF potential for the single-helicity case are plotted in Fig. 1 (left) for $M_p = 0$, 0.1, 0.2 and 0.3, where the radial wavenumber $k_r = k_x = 0.065 \rho_i^{-1}$. For $M_p = 0$, after the initial GAM (geodesic acoustic mode) damping ($t > 15 R_0/v_{ti}$), one finds the residual ZF with the small but constant amplitude of $\langle \phi(t) \rangle / \langle \phi(t=0) \rangle \simeq 0.011$. The zonal flow response is not much altered for $M_p = 0.1$, but clearly grows in time for $M_p = 0.2$, where the ZF amplitude at $t = 30 R_0/v_{ti}$ is about six times higher than that of the residual value for the case of $M_p = 0$. As we have seen in our previous work [26], the response function starts to oscillate in time for the larger M_p, which is related to the periodic motion of trapped particles to the radial electric field.

The simulation results for the inward-shifted model case shown in Fig. 1 (right) demonstrate the enhancement of the residual zonal flow after the collisionless Landau damping of the GAM. The effect of E_{r0} clearly appears even for $M_p = 0.1$, and becomes more prominent for the higher M_p. Indeed, the ZF potential with $k_r \rho_i = 0.065$ for $M_p = 0.3$ at $t = 30 R_0/v_{ti}$ is about 5.7 times larger than that for $M_p = 0$. The time-averaged potential amplitude (from $t = 15$ to $30 R_0/v_{ti}$) is more significantly increased in the inward-shifted case (more than 20 times for $M_p = 0.3$ in comparison to the case for $M_p = 0$), where the residual ZF level is nearly constant in time in contrast to the single helicity case with the oscillatory ZF response.

Here, it should be mentioned that the time-integration of the zonal flow potential during the GAM damping phase ($t < 10 R_0/v_{ti}$) is larger in the inward-shifted model case than that in the single helicity one [13]. This also contributes to the more effective ZF generation in the former [25], in addition to the higher residual levels in the long time limit after the GAM damping in case with E_{r0}.

Radial wavenumber (k_r) dependence of the residual ZF amplitude is investigated for the inward-shifted model case with $M_p = 0$ and 0.3 [see Fig. 2 (left)], where the horizontal line

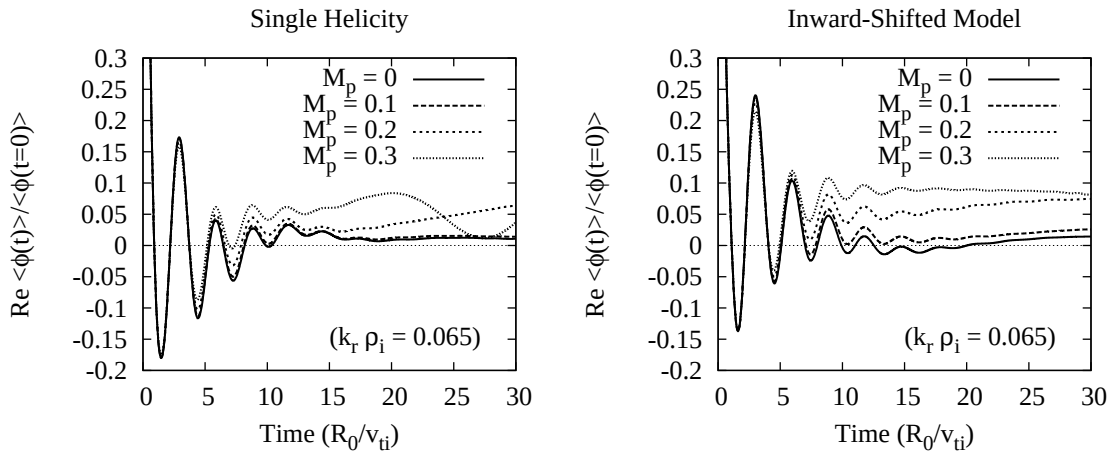

FIG. 1: Time-history of the zonal flow potential for the single-helicity (left) and the inward-shifted (right) model cases with different poloidal Mach numbers of $M_p = 0, 0.1, 0.2$ *and* 0.3.

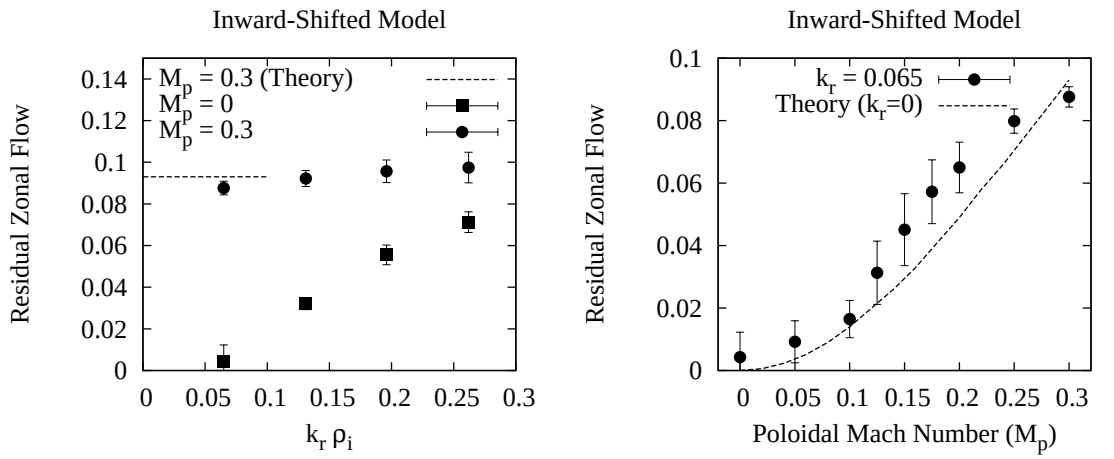

FIG. 2: (Left) Radial wavenumber (k_r) *dependence of the residual zonal flow potential amplitude for the inward-shifted model case with* $M_p = 0$ *(square) and* 0.3 *(solid circle), where* $\phi(t)$ *is time-averaged from* $t = 15$ *to* $30R_0/v_{ti}$. *(Right) Poloidal Mach number* (M_p) *dependence of the residual zonal flow potential amplitude* $\mathrm{Re}\langle\phi(t)\rangle/\langle\phi(t=0)\rangle$ *for the inward-shifted model case with* $k_r\rho_i = 0.065$ *where* $\phi(t)$ *is time-averaged from* $t = 15$ *to* $30R_0/v_{ti}$. *Dashed line shows the theoretical estimate of the residual zonal flow amplitude in the limit of* $t \to \infty$ *for* $k_r\rho_i = 0$.

represents the theoretical prediction in the long wavelength limit [19]. In the case without E_{r0} ($M_p = 0$), the zonal flow response shows a clear k_r-dependence, and the residual level vanishes in the long wavelength limit of $k_r\rho_i \to 0$. The simulation results shown in Fig. 2 (left) for $M_p = 0$ agree with the ZF response predicted by the theoretical analysis [11, 12] even with the field-line-label dependence of the confinement field.

The residual ZF level is largely enhanced by the radial electric field E_{r0}. A qualitative difference from the cases with $M_p = 0$ is found in the small wavenumber region, where the residual flow for $M_p = 0.3$ remains finite in contrast to the case of $M_p = 0$. The residual flow level given by the simulations for $k_r\rho_i = 0.065$ agrees well with the theoretical value shown by the dashed line in Fig. 2 (left). The simulation results manifest that the poloidal rotation enhances the ZF response effectively in the inward-shifted model configuration.

2.4 Isotope Effects on Zonal Flow Response

Poloidal Mach number dependence of the ZF response for $k_r\rho_i = 0.065$ is summarized in Fig. 2 (right), where the residual level increases with M_p in agreement with the theoretical

prediction for $k_r\rho_i \to 0$ (shown by the dashed line). Rapid growth of the ZF response is found for $M_p \sim 0.1$-0.2, where the residual flow for $M_p = 0.15$ is about 2.7 time stronger than that for $M_p = 0.1$. The parameter range for M_p considered here is relevant to the LHD experimental conditions. Specifically, for $B_0 = 2.75$T, $R_0 = 3.6$m, $r_0 = 0.36$m, $q_0 = 2$, $T_i = 5$keV and $E_{r0} =$ 10kV/m, one finds $M_p \simeq 0.1$ and 0.14 for hydrogen and deuterium discharges, respectively. Here, it should be reminded that, for the same T_i and E_{r0}, the M_p-dependence of the ZF response is equivalent to the isotope effect. The present simulation results suggest that, for the fixed E_{r0} and T_i, the ZF response can be enhanced by the heavier ion mass under conditions relevant to the LHD experiments.

3. Gyrokinetic Simulations of Ion Temperature Gradient Instability

To assess the possibility of turbulent transport reduction by the zonal flow enhancement due to the isotope effect in helical systems with E_{r0}, we develop a new GKV code with further extensions of the field-line-label (α) dependence of the confinement field, and apply it to the ITG instability analysis.

3.1 Simulation Model

Since the ITG instability is a microscopic drift wave mode, it is convenient to employ the field aligned coordinates of $x = r - r_0$, $y = (r_0/q_0)\,[q(r)\theta - \zeta]$, and $z = \theta$, in the same manner as that used in the conventional flux tube model. In contrast to the previous section, the field-line-label is defined by $\alpha = \zeta - q\theta$. This choice enables us to set the toroidal (α) period number of simulation box $N_\alpha = M$, and to introduce the finite magnetic shear $\hat{s}$. For perturbed ion gyrocenter distribution function, we solve the gyrokinetic equation with the diamagnetic and the $\boldsymbol{E} \times \boldsymbol{B}$ drift terms, where the α-dependence of the magnetic drift and mirror force terms is included.

3.2 Simulation Results

We first apply the new flux tube code to the linear gyrokinetic simulation of the ITG instability. Figure 3 shows the linear frequency (ω_r) and growth rates (γ) of the ITG instability for $M_p = 0$ and 0.3, where the magnetic field geometry relevant to the inward-shifted LHD configuration [13,25] is employed. Here, we introduced the finite collisionality of $\nu = 2 \times 10^{-3} L_n/v_{ti}$ with the Lenard-Bernstein model collision operator [24] and the magnetic shear $\hat{s}$. As expected, the linear instability growth rates are not influenced by the equilibrium electric field, E_{r0}, while the phase velocity in the laboratory frame is modified. The difference of the real frequency agrees with the Doppler shift due to the equilibrium-scale poloidal $\boldsymbol{E} \times \boldsymbol{B}$ flow. Here, it should be mentioned that the linear growth rates are measured in the early stage of simulation (at $t = 23 L_n/v_{ti}$). In later time, unstable eigenmodes overlap each other, because of the α-dependence of operators in the gyrokinetic equation which involves linear eigenmodes consisting of various poloidal wavenumber (k_y) components.

Nonlinear gyrokinetic simulations of the ITG turbulence have also been performed for the inward-shifted LHD model configuration in case with E_{r0} and the α-dependence of the confinement field strength. Comparisons of the ion heat transport coefficient, χ_i, and the turbulent potential fluctuations T as well as the zonal flow amplitudes Z are, respectively, shown in Figs. 4 (left) and (right) for $M_p = 0$ and 0.3. Here, we define $T = \sum_{\boldsymbol{k}, k_y \neq 0} \langle |\phi_{k_x,k_y}|^2 \rangle / 2$ and $Z = (\sum_{k_x} \langle |\phi_{k_x,k_y=0}|^2 \rangle / 2)^{1/2}$, respectively. In an early nonlinear phase just after saturation of the ITG instability growth ($t \simeq 40$ to $80 L_n/v_{ti}$), one finds reduction of the transport coefficient χ_i and the turbulent fluctuations T for $M_p = 0.3$ in comparison with those for $M_p = 0$. In the longer

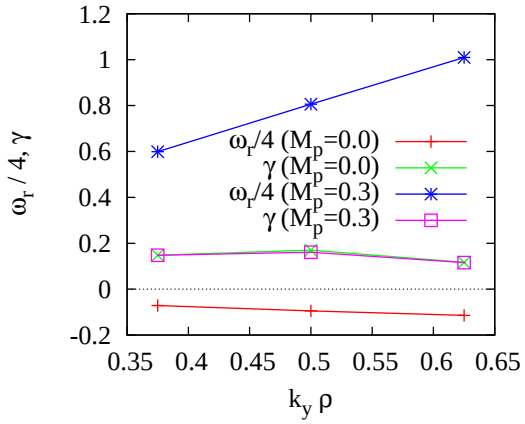

FIG. 3: Linear frequency (ω_r) and growth rates (γ) of the ITG instability for $M_p = 0$ and 0.3, where the finite collisionality of $\nu = 2 \times 10^{-3} L_n/v_{ti}$ and the magnetic shear are included.

time period ($t \simeq 40$ to $300 L_n/v_{ti}$), the time-averaged values of χ_i are 1.21 and 1.10 $\rho_i^2 v_{ti}/L_n$ for $M_p = 0$ and $M_p = 0.3$, respectively. Reduction of the turbulent fluctuations is more clearly found in Fig. 4 (right), where the time-averaged value of T is 6.7 for $M_p = 0$ but is reduced to 5.4 for $M_p = 0.3$ (about 20% reduction).

In the later phase of the simulations with the relatively small box size (that is, $3/5$ of that used in Ref. [25] in the y-direction), dominant low-k_y components often cause large amplitude of fluctuations in the time-evolutions of χ_i as well as the zonal flow amplitudes, which may influence the quantitative estimate of χ_i. Also, the finite ion-ion collision is introduced with the effective collision time of $\tau_{\rm eff} = \nu_{\rm eff}^{-1} \sim (\nu/\varepsilon_h)^{-1} \sim 50 L_n/v_{ti}$ which is only 2.6 times longer than the poloidal rotation time, $\omega_\theta^{-1} = 18.9$, and leads to the collisional damping of residual ZFs. This may provide an explanation for the transport reduction smaller than that expected from the collisionless ZF response enhancement in the previous section. Nevertheless, it should be noteworthy that the turbulent transport reduction in case with $M_p = 0.3$ is clearly found in the early nonlinear phase ($t \simeq 40$ to $80 L_n/v_{ti}$).

In Fig. 5, we plot ratio of the ZF amplitude, Z, and the turbulent fluctuations, T, which can be employed as a measure for effectiveness of the zonal flow generation by turbulence. In the case with $M_p = 0.3$, the ZF amplitude normalized by the turbulent fluctuations (Z/T) increases after the saturation of the instability growth at $t \simeq 40 L_n/v_{ti}$, even though almost the same values of T are found before the saturation. The obtained results suggest that the ZF response enhancement due to the equilibrium-scale radial electric field contributes to the turbulence suppression and the transport reduction.

4. Summary

By means of the gyrokinetic simulations, isotope effects on the zonal flow (ZF) response and the ion temperature gradient instability are investigated for the non-axisymmetric (helical) configurations with the equilibrium-scale radial electric field (E_{r0}). The newly extended GKV code including the field-line-label (α) dependence of the confinement field is utilized for solving the initial value problem of the collisionless ZF damping and the linear ITG instability.

The residual ZF levels apparently show the poloidal Mach number (M_p) dependence, where the ZFs are amplified by E_{r0} in the inward-shifted model case. The obtained M_p-dependence indicates rapid increase of the ZF response in the range of $M_p \sim 0.1$-0.2. The isotope effect on ZF response, thus, appears through E_{r0} generated by the neoclassical transport, and is expected

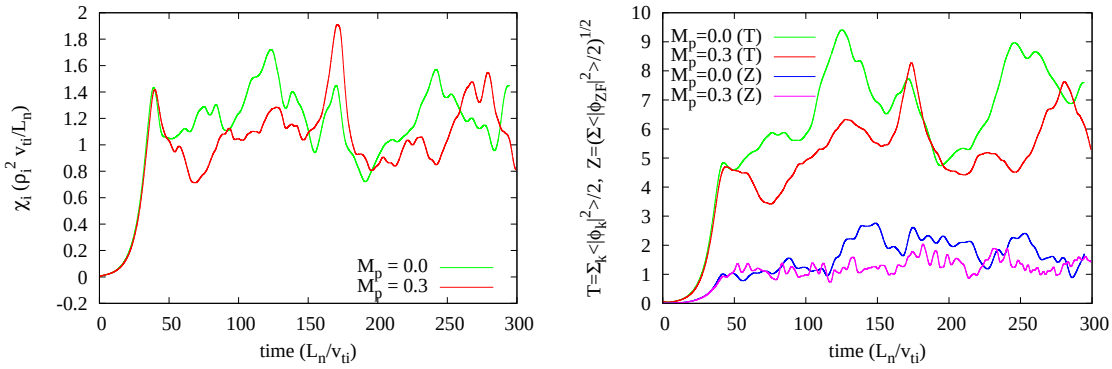

FIG. 4: (Left) Ion heat transport coefficient, χ_i obtained from the nonlinear GKV *simulation of the ITG turbulence for the inward-shifted LHD model configuration in case with E_{r0} and the α-dependence of the confinement field strength. Green and red curves represent the cases with $M_p = 0$ and 0.3, respectively. (Right) Turbulent potential fluctuations $T = \sum_{\boldsymbol{k},k_y\neq 0}\langle|\phi_{k_x,k_y}|^2\rangle/2$ (green and red) and zonal flow potential amplitudes $Z = (\sum_{k_x}\langle|\phi_{k_x,k_y=0}|^2\rangle/2)^{1/2}$ (blue and magenta) for the cases of $M_p = 0$ and 0.3.*

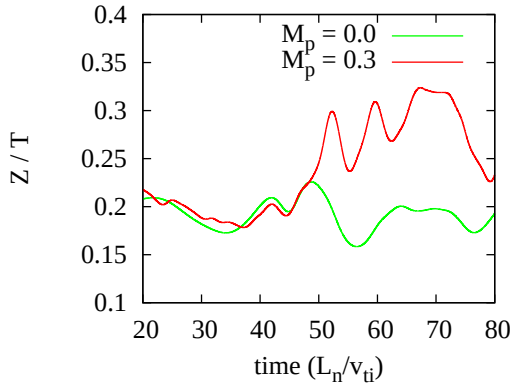

FIG. 5: Zonal flow potential amplitudes normalized by the turbulent fluctuations (Z/T) in an early phase of the simulations for $M_p = 0$ (green) and 0.3 (red).

to play a favorable role in reducing the turbulent transport. The present study on the radial wavenumber (k_r) dependence also confirms the significant amplification of the ZF response in the small $k_r\rho_i$ limit as predicted in the previous works [18–20].

It is also confirmed that growth rates of the linear ITG instability remains unchanged even with the poloidal Mach number of $M_p = 0.3$, while the real frequency is Doppler shifted by the equilibrium-scale poloidal $\boldsymbol{E}\times\boldsymbol{B}$ flow. This means that, if the role of ZFs influenced by E_{r0} are not taken into account, the isotope effect in the ion heat transport due to the ITG modes obeys the conventional gyro-Bohm scaling in case with the adiabatic (mass-less) electron response. A preliminary simulation study of the helical ITG turbulence with E_{r0} suggests more effective ZF generation and turbulence suppression for $M_p = 0.3$ than those for $M_p = 0$.

For helical systems, E_{r0} reducing the radial drift motions of helical-ripple-trapped particles is introduced in the gyrokinetic equation through M_p that is larger with heavier ion mass for the same E_{r0} and T_i. In contrast to axisymmetric configurations, accordingly, the uniform and constant E_{r0} leads to the isotope effect on the ZF response in non-axisymmetric systems, as the magnitude of E_{r0} caused by the neoclassical transport in the deuterium discharge is almost identical to that in the hydrogen plasma in LHD [22]. In addition, the helical field optimization with slower radial drift motion of helical-ripple-trapped particles is known to enhance the ZF response [25]. Couplings of the neoclassical transport causing E_{r0}, the enhanced zonal flows,

and the regulation of ITG turbulence are, therefore, expected to bring the isotope effect on the anomalous transport into helical plasmas. The possibility of turbulent transport reduction by the zonal flow enhancement due to E_{r0} strongly motivates more elaborate simulation studies on the ITG turbulence and ZFs in helical systems with the field-line-label dependence of the confinement field.

Acknowledgments

This work is supported in part by grants-in-aid of the Ministry of Education, Culture, Sports, Science and Technology (No. 21560861 and 22760660), and in part by the National Institute for Fusion Science (NIFS) Collaborative Research Program (NIFS10KTAT040, NIFS10KDAT020, and NIFS10KNXN186). Numerical simulations are carried out by use of the Plasma Simulator system at National Institute for Fusion Science.

Reference

[1] ITER Physics Expert Group 1999 *Nucl. Fusion* **39** 2175
[2] Diamond P H, Itoh S I, Itoh K and Hahm T S 2005 *Plasma Phys. Control. Fusion* **47** R35
[3] Horton W 1999 *Rev. Mod. Phys.* **71** 735
[4] Dimits A M, *et al* 2000 *Phys. Plasmas* **7** 969
[5] Rosenbluth R M and Hinton F L 1998 *Phys. Rev. Lett.* **80** 724
[6] Hinton F.L. and Rosenbluth M.N. 1999 *Plasma Phys. Control. Fusion* **41** A653
[7] Xiao Y. and Catto P.J. 2006 *Phys. Plasmas* **13** 082307
[8] Kim E.J. *et al* 2003 *Phys. Rev. Lett.* **91** 075003
[9] Xiao Y. and Catto P.J. 2006 *Phys. Plasmas* **13** 102311
[10] Sugama H. *et al* 2007 *Phys. Plasmas* **14** 022502
[11] Sugama H and Watanabe T H 2005 *Phys. Rev. Lett.* **94** 115001
[12] Sugama H and Watanabe T H 2006 *Phys. Plasmas* **13** 012501
[13] Ferrando-Margalet S, Sugama H and Watanabe T H 2007 *Phys. Plasmas* **14** 122505
[14] Mynick H E and Boozer A H 2007 *Phys. Plasmas* **14** 072507
[15] Mishchenko A, Helander P and Könies A 2008 *Phys. Plasmas* **15** 072309
[16] Yamagishi O and Murakami S 2009 *Nucl. Fusion* **49** 045001
[17] Landremen M and Catto J 2010 *Plasma Phys. Control. Fusion* **52** 085003
[18] Sugama H, Watanabe T H and Ferrando-Margalet S 2008 Plasma Fus. Res. **3** 041
[19] Sugama H and Watanabe T H 2009 *Phys. Plasmas* **16** 056101
[20] Sugama H, Watanabe T H and Nunami M 2010 *Contrib. Plasma Phys.* **50**, 571-575
[21] Motojima O, *et al* 2003 *Nucl. Fusion* **43** 1674
[22] Yokoyama M, *et al* 2010 *Contrib. Plasma Phys.* **50**, 586-589
[23] Watanabe T H and Sugama H 2006 *Nucl. Fusion* **46** 24
[24] Watanabe T H, Sugama H. and Ferrando-Margalet S. 2007 *Nucl. Fusion* **47** 1383
[25] Watanabe T H, Sugama H and Ferrando-Margalet S 2008 *Phys. Rev. Lett.* **100** 195002
[26] Watanabe T H, Sugama H. and Ferrando-Margalet S. 2008 *Proceedings of the 22nd IAEA Fusion Energy Conference* (Geneva, Swiss Confederation) TH/P8-20
[27] Kleiber R, Hatzky R and Mishchenko A 2010 *Contrib. Plasma Phys.* **50**, 766-769